

Metering of the Oil and Natural Gas System Emissions using Aerial Site Measurement

Best Eromosele Agbi

Department of Mechanical Engineering
University of Agriculture, Makurdi, Nigeria

doi: <https://doi.org/10.37745/ijeer.13/vol12n1118>

Published March 24, 2024

Citation: Agbi B.E. (2024) Metering of the Oil and Natural Gas System Emissions using Aerial Site Measurement, *International Journal of Energy and Environmental Research*, 12 (1), 1-18

ABSTRACT: *Aerial methane surveys of oil and natural gas systems have discovered large emissions, which are missing or vastly undercounted in official estimates. We integrate approximately one million aerial site measurements into regional emissions inventories, employing empirically grounded emissions simulations to estimate small emissions. We infer emissions inventories for six regions in the United States comprising 52% of onshore oil and 29% of gas production over fifteen aerial campaigns. Total estimated emissions range from 9.63% [9.03%, 10.37%] of natural gas production, roughly nine times the US government estimate, to 0.75% [0.65%, 0.85%] in a high-productivity gas-rich region. Aerially measured emissions at 0.05%-1.44% of well sites contribute 50%-81% of total emissions in twelve of fifteen campaigns. The social cost of methane emissions from these measured regions is roughly \$9.4 billion per year, in addition to roughly \$1 billion in lost sales. This highlights the importance of incorporating comprehensive remote sensing surveys into emissions inventories and efforts to benchmark and reduce methane emissions.*

KEYWORDS: metering, oil, natural gas system, emissions, aerial site measurement

INTRODUCTION

Accurately estimating methane emissions from the oil and natural gas sector is vitally important for mitigating climate change. Current global inventories estimate oil and gas sector emissions of 84 Tg(CH₄)/yr [72, 97] 1. These emissions represent 16% of global anthropogenic greenhouse gas emissions from fossil fuels assuming a 20-year global warming potential 1–3. However, this estimate, and all estimates like it, rely on coarse emission factors used with often-incomplete data. Many countries simply leverage the most general emission intensities from – for example – the United States Environmental Protection Agency’s Greenhouse Gas Inventory, or GHGI 4,5. In the last decade, efforts in the scientific literature have scaled actual ground measurements at up to ~1,000 sites to estimate industry-wide emissions, finding that emission factor approaches like the above can undercount actual emissions by as much as 40% 6. Even more recently, aircraft-based technologies have enabled a 1,000-fold increase in the

size of surveys and have found very large emissions sources. The results of these aerial surveys have not been incorporated into previous systematic inventories because no method existed to combine aerial measurements of large emission sources with inventory methods for smaller sources. In this paper, we close this gap by making a first estimate of large-scale comprehensive emissions across major producing regions by merging results of approximately 1 million site visits with an empirically-grounded statistical model of smaller emission sources. 6,7.

In the 1990s, countries across the world began producing systematic inventories of emissions of methane and other greenhouse gasses to track progress toward climate goals 8. Many national inventories rely on scaling up relatively small datasets of component-level measurements, with underlying empirical data collection often conducted decades ago in the United States 8,9. Rutherford et al. recently demonstrated that updating the underlying component-level data to include the most recent studies largely reconciles these emission factor methods with the ground measurement literature 5.

However, recent remote sensing surveys conducted by airplanes and satellites have discovered a substantial number of point-source methane emissions that are up to three orders of magnitude larger than those reported by ground-based well site methane surveys 10–18. In at least some cases, these low-probability but high-consequence sources can contribute the majority of methane emissions from an oil and gas producing region 13,14. Because ground-based surveys remained dominant in the literature throughout the 2010s, these remote sensing results suggest that emission factor methods such as the GHGI produce an even more significant undercount of total methane emissions than previously thought 6.

Therefore, accurately characterizing the statistical distribution of methane emissions from the oil and gas system, including the likelihood of low-probability, high-emission events – sometimes termed “super-emitters” – is key to accurately estimating total methane emissions from an oil and gas-producing region 7,19–22. Ground-based methods are inherently challenged to find these due to the low probability of occurrence at a given site and small sample sizes of ground campaigns.

In order to make regional estimates including data from airplane-based point-source sensing methods, we need to understand emissions distributions both above and below the detection limit of the technology in question. Understanding the full distribution of methane emissions is also necessary when evaluating equivalence between different emission detection and mitigation programs. A theoretical basin dominated by large emissions will benefit from a scalable approach, such as airborne, that can rapidly detect large sources, while another basin with most methane lost to smaller emissions will be more effectively surveyed by ground-based or other high-sensitivity approaches. Note that while airplane-based area flux estimation methods can produce regional estimates that do not attribute emissions to sources 6, this study focuses on airplane-based point source methods, which can detect individual sources at the facility level.

Air- or ground-based surveys each necessarily miss some emissions. However, quantifying that missing amount is a challenge. Ground-based surveys can see most sources reliably, although they may miss elevated sources such as tanks and flares 23, but are slow and expensive and therefore are generally limited to small sample sizes of tens to hundreds of sites. This limited sampling potentially misses large, low-

probability emissions. In contrast, aerial surveys can cover vast swaths of landscape, but have a higher minimum detection limit that prevents them from seeing smaller sources. Thus, these two methods each exhibit complementary strengths and weaknesses, but past work has had difficulty reliably to synthesize these disparate results into a complete distribution of methane emission rates. Johnson et al. take steps in this direction, combining aerial measurements with emissions simulation methods for 8% of well sites in British Columbia 24.

In this paper we develop an approach to construct such a complete distribution, from the smallest to the largest sources at the regional scale, leveraging comprehensive aerial surveys as well as a state-of-the-art component-level emission simulation tool 5. We define a comprehensive survey as including measurements of at least 50% of well sites and 80% of natural gas production in a region. Such region-specific distributions can inform methane emissions inventory development and guide deployment of methane-sensing technologies whose spatial coverage and detection limits most closely match the needs of a particular area.

A key challenge in combining data from various methods is avoiding errors when datasets are joined. For example, data generated should cover the entire range of expected emission sizes, avoiding gaps at intermediate sizes. Also, one must avoid double-counting emission prevalence where two methods may both be able to see emissions of a given size. Another significant consideration is ensuring the surveyed area has an emissions profile that is representative of the area of interest, e.g. an entire oil and gas-producing basin. We describe below an approach that combines emissions simulation and aerial measurement methods into a single distribution, avoiding double-counting and mitigating data gaps in intermediate size ranges for all assets within a surveyed area.

We generate a unified methane emissions distribution for surveyed oil and gas assets in six US oil and gas producing regions: the Permian, San Joaquin, Denver-Julesburg, Uinta and Fort Worth basins, and Appalachian Pennsylvania.

Eleven of these are comprehensive, with the Pennsylvania and Permian 2020 and 2021 campaigns still covering at least 10% of well sites and 39% of natural gas production. These surveys include 959,573 well site measurements as well as a difficult-to- quantify number of measurements of midstream infrastructure, including compressor stations, gas processing plants, and pipelines. The surveyed areas within these regions comprise 29% of onshore US gas production and 52% of oil production. We combine fifteen large aerial surveys, conducted by Kairos Aerospace (Kairos) and researchers leading the Carbon Mapper (CM) project, with an empirically- grounded emissions simulation method introduced in Rutherford et al. 2021. We refine this model with input parameters based on regional characteristics, and estimate small-source midstream emissions based on state-level and national GHGI data . Given proper input data, this emissions simulation method produces results that largely reproduce the distribution of site-level emissions from a synthesis of the ground-based site-level methane measurement literature . We demonstrate that our combined emissions distribution is consistent with major ground-based and aerial methane measurement studies.

Uniting Aerial Measurement with Simulated Emissions

For all oil and gas production assets covered in each surveyed region, we compute two well site-level emissions inventories: One based on aerial measurements and the other using the Rutherford et al. emissions simulation tool. We consider a well site to be a point location that may contain multiple wells and supplementary equipment such as liquids tanks, flares, and separators.

Figure 1B provides a high-level overview of the 1000-realization Monte Carlo-based method we use to synthesize these two emissions inventories into a unified estimate of the distribution of methane emissions across surveyed well sites, which allows estimation of total emissions.

Aerial surveys also cover midstream assets such as gathering and transmission pipelines, compressor stations, and gas processing plants. We estimate aerially measured and partially detected midstream emissions using the same approach as above. We do not have sufficient asset location data or emissions simulation tools for midstream infrastructure to estimate site-level emissions below the aerial detection limit. We instead estimate these emissions based on the EPA national and state-level GHGI, removing the fraction of emissions underlying those estimates that would be detectable by Kairos or CM 9,25. All Kairos data used in this study are fully anonymized, and include no identifying information for covered operators or their assets. See Materials and methods for further detail.

Estimation at the site-level, rather than site-visit level, is key. Treating each aerial site visit as a completely independent measurement can introduce significant bias if a subset of assets that is not representative of the full survey area is disproportionately over-sampled, as demonstrated in the Supplementary Information (SI), Section S8. Note that we do not estimate methane emissions from local distribution or oil refining and transportation, which occur at facilities largely outside the surveyed regions.

Methan Loss rates vary widely Over Space and Time

Estimated methane loss rates – the emitted fraction of methane produced from oil and natural gas activity in a given region – vary widely across the studied US regions. Estimated rates are as low as 1.08% [0.98%, 1.18%] in the Denver-Julesburg basin in Colorado in 2021, and 0.75% [0.65%, 0.85%] in a high-productivity area of the Pennsylvania portion of the Appalachian basin, as shown in Figure 2. In contrast, for the New Mexico Permian 2018-2020 campaign, the loss rate is 9.63% [9.03%, 10.37%], an order of magnitude higher. The remaining campaigns range from roughly 2% to 6% methane loss rates. The production-weighted loss rate across all fifteen campaigns is 2.97% [2.78%, 3.18%], rising to 4.77% [4.51%, 5.07%] excluding the four campaigns focusing on high-productivity sub-regions. These loss rates assume a conservatively high methane fraction of 90% from 6. If the actual methane fraction is lower, these loss rates would increase correspondingly, as discussed in the SI, Section S7.

Most of these estimates are far larger than the national EPA GHGI, which places the 2020 US-wide onshore methane loss rate at 1.01% [0.81%, 1.22%], after excluding municipal distribution systems, crude oil transportation and refining, and post-meter emissions for consistency with this study 9. These loss rates

also generally exceed state-specific EPA inventories, shown as dotted lines in Figure 2, although these estimates roughly align in the Denver-Julesburg and the studied region of Pennsylvania, and the EPA value actually exceeds our estimate for four of the five San Joaquin campaigns 25. See the Materials and methods for further description of our treatment of EPA GHGI estimates.

Multiple surveys across the oil-focused San Joaquin and Permian basins demonstrate substantial variation in loss rates over time. The five San Joaquin campaigns find loss rates as low as 2.52% [2.20%, 2.87%] in fall 2021, and as high as 5.56% [4.97%, 6.23%] in 2017. All San Joaquin campaigns cover at least 80% of the basin's gas production and over 80% of all actively producing well sites. Across the Permian 2020 and 2021 campaigns, which cover similar areas, the methane loss rate varies from 2.10% [1.94%, 2.27%] to 2.81% [2.59%, 3.05%].

Even large surveys of the same region can produce divergent results if they cover different areas. Loss rates in the five Permian campaigns vary from 2.10% [1.94%, 2.27%] in the fall 2021 campaign, focusing on high-productivity areas, to 9.63% [9.03%, 10.37%] in the New Mexico Permian from 2018-2020. The largely overlapping 2019 survey of both Texas and New Mexico finds 5.29% [5.07%, 5.51%]. See the SI, Sections S5 and S12 for further detail.

This area-specific variation highlights the need to use comprehensive, or at least representative, aerial surveys when estimating regional emissions. For this reason, Figure 2 uses semi-transparent bars to represent methane loss rate estimates from the Permian 2020 and 2021 campaigns, as well as the Pennsylvania 2021 campaign, all of which disproportionately focus on high-productivity areas and cover less than 80% of natural gas production and less than 50% of well sites in the region in question. For simulated well site emissions, we account for the productivity of surveyed well sites, as described in the SI, Section S1.4 and S13, but this simply improves the fidelity of simulated emissions within the covered region. As a result, our estimates from these less comprehensive campaigns should not be extrapolated to the full region (e.g. the entire Permian basin or all of Pennsylvania, respectively).

In all cases, midstream emissions are a significant fraction of the total. Midstream emissions represent 45%-57% of total estimated oil and gas emissions in the Permian basin. This falls to 31%-55% in the San Joaquin basin and 18% in the Uinta. We estimate midstream emissions at 32-37% of the total in the Denver-Julesburg basin, although aurally measured midstream emissions are only 3-10% of the total, suggesting that simulated midstream emissions may be an overestimate in this case. See Materials and methods for further discussion of simulated midstream emissions, which are derived from the national and state-level GHGI reports 9,25.

Note that campaigns in the same region with comparable well site coverage may cover different amounts of midstream infrastructure, which may affect estimated midstream emissions estimates. We do not have sufficient midstream asset location data to quantify this effect here. See the SI, Section S12 for coverage information for each campaign.

Aerial Measurement Often Dominate Total Emissions

Aerially measured emissions play a major role in nearly all basins, contributing 50-81% of the total in all Permian, San Joaquin, Pennsylvania, and Fort Worth campaigns. This rises as high as 84% in the New Mexico Permian after accounting for missed emissions in the partial detection range of the aerial system. The fraction of aerially measured emissions falls to 41% the Uinta, and 14-20% in the Denver-Julesburg. Note that this does not include emissions below the transition point from simulated to aerially measured emissions, which excludes some emissions in the partial detection range if simulated emissions are larger. This means that the fraction of emissions that is aerially detectable is even greater, as illustrated in the SI, Section S3.

Many new methane-sensing technologies have emerged in the past several years. To assess the fraction of total emissions that a technology with a given sensitivity would see in each region, we show the full well site-level emissions distribution for all actively producing well sites covered in each of the fifteen campaigns in Figure 3. Note that these distributions do not include midstream emissions, as we do not have site-level simulated emissions estimates in that case. Each point on these distributions represents a well site emission magnitude, on the x-axis, and the fraction of total estimated regional emissions coming from well sites emitting at least that amount on the y-axis.

Despite their substantial contribution to the total in all cases, aerially detected emissions are present at only a small fraction of sites at a given time. In the Permian basin, an average of 0.86%-1.44% of total well sites are emitting in a given Monte Carlo simulation. This fraction falls to 0.05%-0.09% of sites in the San Joaquin, with the remaining regions between the two. Thus, while previous literature focused on ground-based measurements found that 5% of measurements often contributed 50% of total emissions 21, this study finds that less than 1% of measurements contribute over 50% of total emissions in 12 of 15 cases. See the SI, Section S2 for further discussion of the shape of the emissions distribution, which generally resembles a lognormal for simulated emissions and a power law for aerially measured emissions.

For Kairos datasets, we use single-blind controlled release test results to correct for missed emissions in the partial detection range (teal in Figure 2 and Figure 3). If the probability of detecting an emission of a certain magnitude is $1/3$ and such an emission is detected, this implies that two emissions of comparable magnitude were likely missed by the survey. Thus, we account for this in the cumulative emissions distribution by multiplying the contribution of this emission to the total by 3, as described in the SI, Section S1.7. Note that due to the required use of wind reanalysis data, the high end of the partial detection range for Kairos is larger than observed when using in situ field wind measurements, as in 26.

The point at which each distribution transitions from simulated to aerially measured emissions is often at a higher rate than the smallest aerially measured emission. We set this transition point as the site-level emission magnitude beyond which aerially measured emissions are larger than simulated emissions (described further in the SI, Sections S1.8 and S3). As a result, some small emissions detected in most campaigns are not included in the combined distribution. This is likely because they fall within the partial detection range of the system, which can vary depending on the sensitivity of the sensor, flight altitude,

automated and manual quality control processes, and local environmental conditions such as wind, sun angle, surface reflectance, and vegetation cover. While we correct for missed emissions in the partial detection range for Kairos surveys using the method from 13, commensurate single-blind controlled release testing data to do so for Carbon Mapper. In addition, Carbon Mapper conducted flights at different altitudes across campaigns, as described in the SI, Section S12, affecting the lower detection range.

The absence of a correction in the partial detection range for Carbon Mapper campaigns, coupled with variation in detection capabilities introduced by flight altitude and other above-mentioned factors, likely explains the somewhat higher transition points observed compared to Kairos campaigns. In the San

Joaquin and Pennsylvania distributions, relatively flat areas indicate a gap between the largest simulated emissions and the smallest measured emissions, suggesting our estimates of total emissions in these regions may be conservative, due in part to missing emissions in this middle size range that exist but were not captured by our method. Carbon Mapper personnel believe that the gap in Pennsylvania is partially due in part to high vegetative cover. In probability density function form, shown in the SI, Section S2, this gap between simulated and measured emissions appears as a local minimum in emission frequency, generally ranging between 10 kg/hr and 100 kg/hr, followed by a local maximum for aurally measured emissions. It is unclear whether the underlying distribution has a true local minimum in this size range in some regions, or whether this is entirely an artifact introduced by sensor minimum capabilities.

In some cases, aurally detectable emissions significantly exceed the aurally measured portion of the combined distribution. The vertical lines in Figure 3 represent the minimum emission detected by each aerial technology in each region. In some instances, this is close to the transition point, as in the Kairos New Mexico Permian campaign, which has a minimum detected emission of 7 kg/hr and a transition point of 19 kg/hr. This indicates that while aurally measured emissions contribute 83% of total emissions, Kairos-detectable emissions constitute 88%. The gap is larger for the Denver-Julesburg, where aurally measured emissions are 14% of the total and Carbon Mapper-detectable emissions are 45% of the total. While some of these detectable emissions may lie in an aerial technology's partial detection range, this illustrates that the distributions in this paper provide a conservative estimate of the fraction of emissions these technologies will see when deployed in the field.

Regions with high emission rates are not necessarily dominated by aurally measured emissions. In the Uinta, aurally measured emissions comprise a relatively small fraction of total production site emissions, 41%, even though the overall methane loss rate is the second highest of all campaigns. In this case, production site simulated emissions alone constitute a 3.00% [2.86%, 3.13%] methane fractional loss rate, including only emissions below the transition point of 52 kg/hr. A major reason for these large simulated emissions in the Uinta basin is the widespread use of emission-prone gas-driven pneumatic controllers, shown in more detail in the SI, Sections S1.4.2 and S4. This illustrates the importance of capturing regional variability in well site composition when simulating emissions. See the SI, Section S3 for full aerial and simulated distributions for each campaign.

Code availability

The data and code required to reproduce the key results of this article, as well as 100,000 random samples from each simulated emissions distribution in this study, are available at <https://github.com/esherwin/MethaneDistributions>.

Data availability

The remaining Kairos Aerospace data from this study are not available for open release due to confidentiality concerns, Kairos Aerospace is committed to working with research groups studying methane emissions.

METHODS

We estimate the full distribution of the magnitude of methane emissions for 15 large-scale aerial surveys of at least 10% of well sites and at least 35% of natural gas production in each of six regions, although the Pennsylvania survey covers only 8% of statewide oil production. This includes campaigns by Kairos in the New Mexico Permian basin and the Fort Worth basin in Texas (focusing on the Barnett shale), alongside campaigns conducted by the Carbon Mapper-led team (including scientists from JPL, the University of Arizona, and Arizona State University) in the Permian basin in New Mexico and Texas campaigns), California's San Joaquin basin (5 campaigns), the Denver-Julesburg basin (2 campaigns), as well as the Uinta basin and a high-productivity portion of the Appalachian basin in Pennsylvania (1 campaign each) 10,12,33–35.

All campaigns use hyperspectral infrared spectroscopy to detect and quantify methane emissions using the spectral signature of methane in reflected sunlight. The quantification accuracy and minimum detection capabilities of the Kairos technology was independently validated in single-blind controlled release testing in 26. See 36 for further detail surrounding the technology. The Carbon Mapper campaigns were conducted with the Airborne Visible-Infrared Imaging Spectrometer - Next Generation (AVIRIS-NG) spectrometer on a JPL-contract King Air B200 aircraft and an identical very short wavelength infrared (VSWIR) imaging spectrometer on the Global Airborne Observatory (GAO) operated by Arizona State University, both described in 12. The AVIRIS-NG and GAO systems have also undergone non-blinded controlled release testing to assess minimum detection limits and quantification accuracy.

Both teams use data from imaging spectrometers to estimate methane flux rates based on measured atmospheric methane enhancements, retrieved from spectral radiances, combined with estimates of 10 m wind speeds from reanalysis products. For Kairos Aerospace, we combine reported wind-normalized emission rates with HRRR hourly instantaneous wind speed estimates, as in 13. Carbon Mapper uses the average HRRR from the nearest nine reported grid values, averaged over the hour before, hour after, and hour of a given measurement, as described in 10.

Kairos flights were conducted at roughly 900 meters above ground level. Carbon Mapper flights range from 3,000 meters to 8,500 meters, described in detail in Table 18.

Below we describe the steps to construct a complete emissions distribution from a comprehensive aerial measurement campaign:

To produce an aerial measurement-based regional emissions inventory for oil and natural gas production and midstream activity, one must first conduct a comprehensive aerial survey of the region in question. In this study, we term a survey “comprehensive” if it covers at least 50% of all active oil and natural gas well sites and at least 80% of natural gas production in the region in question, generally an oil and natural gas-producing basin. While future studies may use alternative definitions of “comprehensive”, it is noteworthy that measurement campaigns that focus only on high-productivity or low-productivity areas of a region can produce misleading estimates of the overall regional methane loss rate, as illustrated in the SI, Section S5.

We first estimate the distribution of measured emissions in each aeri ally surveyed region as a function of emission size, using each emission source as the unit of analysis.

potential emission source. In midstream, facilities such as compressor stations and gas-processing plants are potential emission sources, as are pipelines. For pipelines, each detected emission location is considered an emission source.

In many instances, an emission source was surveyed multiple times, with emissions detected during only a fraction of aerial measurements. To account for this, we apply Monte Carlo simulation to characterize the emission profile of the surveyed region. We simulate emissions from each emission source with at least one detected emission, drawing randomly from all aerial measurements at that location, including those with no detected emissions. We then randomly insert simulated error into each quantified emission, based on estimates of quantification uncertainty, discussed further in the SI, Section S1.1. We repeat this stochastic process for 1000 Monte Carlo realizations to capture uncertainty. This method yields an unbiased estimate of total well site emissions in the surveyed region, as described in Chen, Sherwin et al. 2022 13. By analogous logic, it also yields an unbiased estimate of the size distribution of aeri ally visible emissions, but not the variance of total emissions. See the SI, Section S12.2 for further detail. The resulting emissions inventory covers only aeri ally detected emissions, treating emissions as zero at all sites at which emissions were not detected.

In the Kairos Fort Worth survey, 8.5% of detected emission plumes extended beyond the spectrometer’s field of view, and were thus classified as “cutoff” and not quantified. We estimate emission magnitude for these emissions by drawing randomly from the distribution of quantified emissions for well sites and midstream infrastructure, respectively. The number of emission source measurements is not reported for 10 of 11 pipeline emissions in the Kairos Fort Worth survey, out of 72 identified emission sources. We assume these emissions are fully persistent, setting the number of measurements equal to the number of detected emissions at that source.

For emissions approaching the minimum detection level of an aerial detection system, there may be a fractional probability of detection. If an aerial survey of a population of assets detects an emission of a

size that corresponds to a known probability of detection of 1/3, that implies that the survey likely missed two emissions of similar size. Thus, an aerial survey will tend to underestimate emissions in this partial detection range by a predictable amount.

We correct for this effect in the Kairos surveys in the New Mexico Permian basin and the Fort Worth basin, using probability of detection curves based on controlled release testing from. See Materials and methods and the SI, Section S1.7 for further detail.

Carbon Mapper has conducted internal controlled release testing to characterize its minimum detection range. However, we do not have sufficient single-blind controlled release data to apply a similar correction to Carbon Mapper surveys, many of which were also conducted at varying altitudes, further changing lower detection characteristics. This introduces conservatism into estimates of aeri ally measured emissions from Carbon Mapper campaigns.

We then produce a comprehensive well site-level emissions inventory for the surveyed region, as the basis for estimating emissions missed by the aerial survey. We simulate emissions at all surveyed well sites using a basin-scale emissions simulation tool, introduced in. The bottom-up emissions simulation begins with field measurements of the prevalence and magnitude of emissions at the component level, e.g. valves, flanges, and open-ended lines. It then converts these into probabilistic equipment-level emission factors based on component counts for different types of equipment, e.g. separators, meters, and wellheads.

We update this simulation tool with basin-specific equipment activity data from the EPA's Greenhouse Gas Reporting Program, e.g. the number of wellheads and pneumatic controllers per site in a given productivity range, as well as production data, to probabilistically estimate emissions at each well site in a given basin. This analysis thus estimates well site-level emission rates for all surveyed active oil and gas well sites in the six basins.

Simulated well site emissions are based on component-level measurements of methane emission frequency and magnitude, combined with counts of the number of each relevant component (e.g. valves, connectors, and open-ended lines) per piece of well site equipment (as listed in the previous paragraph). Eqs. (1) and (2) summarize the underlying mathematics behind this probabilistic emissions estimation method for a given basin, described in detail in the SI, Section S1.4 and 5.

Where Q_i is simulated emissions for a given simulated well, i , and Q_{basin} is methane emissions from all well sites across the oil and gas-producing basin in question. The i index iterates across all wells in the basin, totalling n_{wells} . The j index iterates across equipment types, with a total of n_{equip} types. $Q_{i,j}$ is a randomly-generated equipment-level emission factor for equipment type j at well i , drawing upon empirical measurements of component counts per piece of equipment, the fraction of components emitting at a given time, and component-level emission rates per emission, described further in the Rutherford et al. 2021 and in the SI, Section S1.4 5. is an equipment activity factor (equipment count per well), drawn from EPA GHGRP data for the basin containing the simulated region. Finally, wells are translated into

well sites using the spatial clustering algorithm introduced in 6. The result is a distribution of well site-level emissions based on the Q_i values.

We identify the number of wells surveyed in a given campaign by filtering the Enverus coordinates of all active wells in the relevant basin by each aerial survey area 38. Enverus does not divide wells into well sites. We convert this count of wells to a count of well sites, assuming the average number of wells per site for the basin, derived from the basin-specific emissions simulation model results, which using the well-to-site clustering algorithm introduced in 6. See the SI, Section S1.6 for further detail.

To account for differences in well site productivity between the surveyed area and the basin as a whole, for each campaigns we draw simulated emissions for each surveyed well site from a well site with similar natural gas productivity. This ensures that simulated emissions are representative of the surveyed area, but does not guarantee that the overall emissions estimate from the surveyed area will be representative of the basin as a whole. See the SI, Sections S13, S1.5, S5 for further detail. The result is simulated emission levels for all well sites covered by each aerial survey.

Sector (MMt/yr)	2016	2017	2018	2019	2020
Gathering & Boosting	1.46	1.53	1.55	1.6	1.5
Processing	0.45	0.46	0.48	0.51	0.49
Transmission & Storage	1.53	1.46	1.54	1.58	1.63
	3.44	3.45	3.57	3.68	3.62
	3.67	3.71	3.66	3.64	3.47
	7.11	7.16	7.23	7.32	7.09
	581	600	672	735	730
	1.2	1.2	1.1	1.0	1.0
	[1.0, 1.5]	[1.0, 1.4]	[0.9, 1.3]	[0.8, 1.2]	[0.8, 1.2]
NG Total (from exploration to post-meter)	6.61	6.66	6.87	6.89	6.6
Oil Total (from exploration to post-meter)	1.62	1.62	1.54	1.62	1.61
Oil & NG Total	8.23	8.28	8.42	8.5	8.21
	1.3	1.2	1.1	1.0	1.0
	[1.0, 1.5]	[1.0, 1.5]	[0.9, 1.3]	[0.8, 1.3]	[0.8, 1.2]

We do not have a site-level emissions simulation tool for midstream infrastructure, comparable to the above well site emissions simulation method. We rely on national and state-level Greenhouse Gas Inventory (GHGI) estimates from the United States Environmental Protection Agency (EPA), which includes reported annual values from 2016 through 2020 9,25. These estimates are based on similar emissions simulation methods.

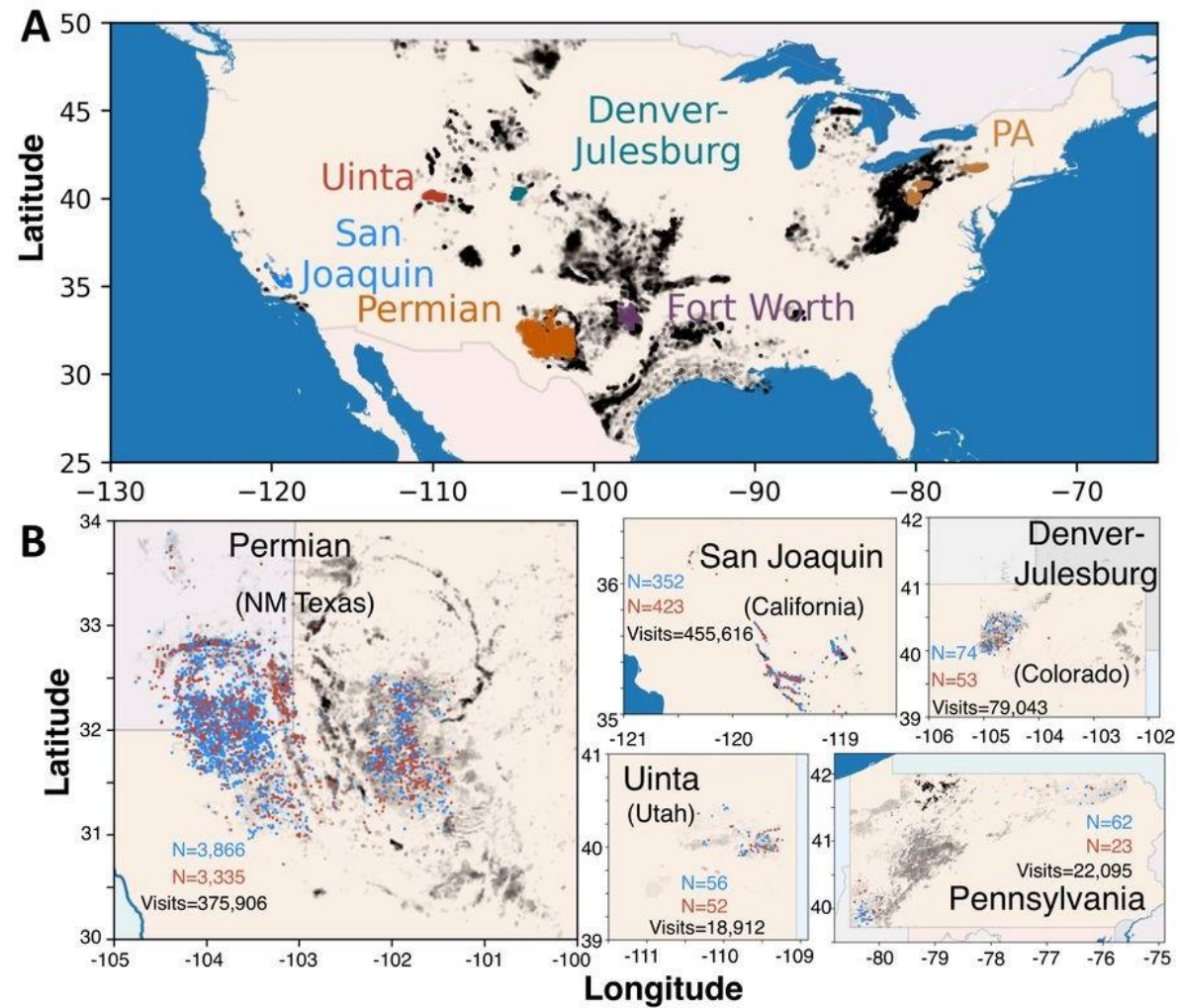
EPA's national inventory includes itemized national emissions from petroleum and natural gas systems. We consider midstream emissions to include EPA's categories of Gathering and Boosting, Processing, and Transmission and Storage.

National methane emissions from oil and natural gas by sector in the United States from the 2022 EPA Greenhouse Gas Inventory in millions of metric tons of methane per year 29. Includes national onshore methane production from onshore oil and natural gas activity from Enverus 38. National methane fractional loss rate estimates include $\pm 18\%$ error for natural gas system emissions and $+32\%/-28\%$ error for petroleum systems, derived from reported uncertainty in 2020 29.

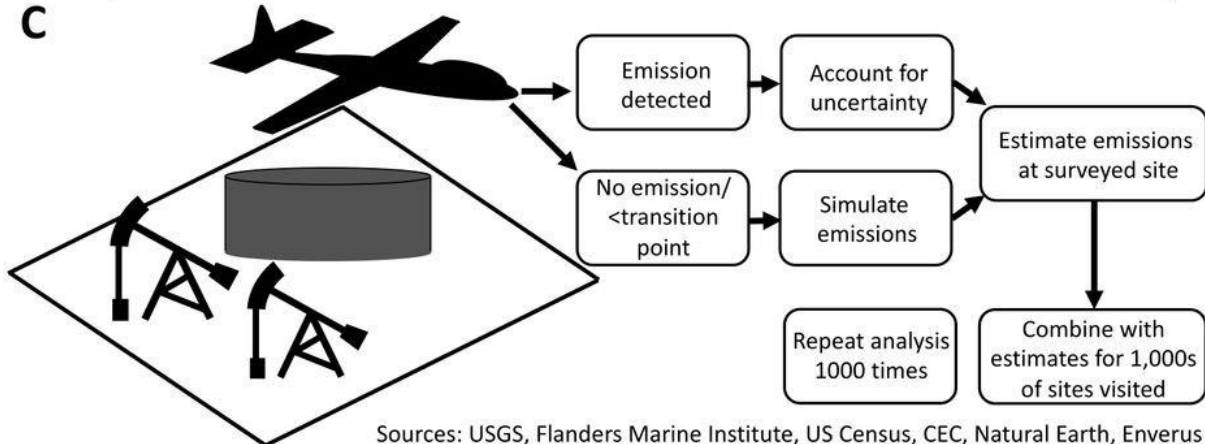
The GHGI also produces state-level emissions inventories 25. These include estimates of total methane production from natural gas systems and petroleum systems, without itemizing midstream and production emissions. For each state, we compute the methane fractional loss rate from natural gas systems by dividing by the state-level GHGI estimate by statewide production from Enverus in the corresponding year, again assuming a 90% methane fraction 6,38.

We then estimate the methane fractional loss rate from midstream infrastructure in each state by assuming that midstream emissions represent the same fraction of total emissions in each state as they do nationally, 42-44% from 2016-2020 6,29. To ensure a conservative estimate, if this value is larger than the national midstream methane fractional loss rate, we use the national rate instead. See for estimated natural gas system and midstream fractional loss rates for each state covered in this study. All cases except the CM Permian campaigns cover only one state. In the CM Permian campaigns, we use the midstream methane fractional loss rate from Texas, as this constitutes most assets surveyed. See 2 for a mapping between each campaign and the state used to estimate the midstream methane fractional loss rate.

Statewide methane emissions from oil and natural gas systems for each campaign from the EPA state-level greenhouse gas inventory. Combined with state-level onshore natural gas production from



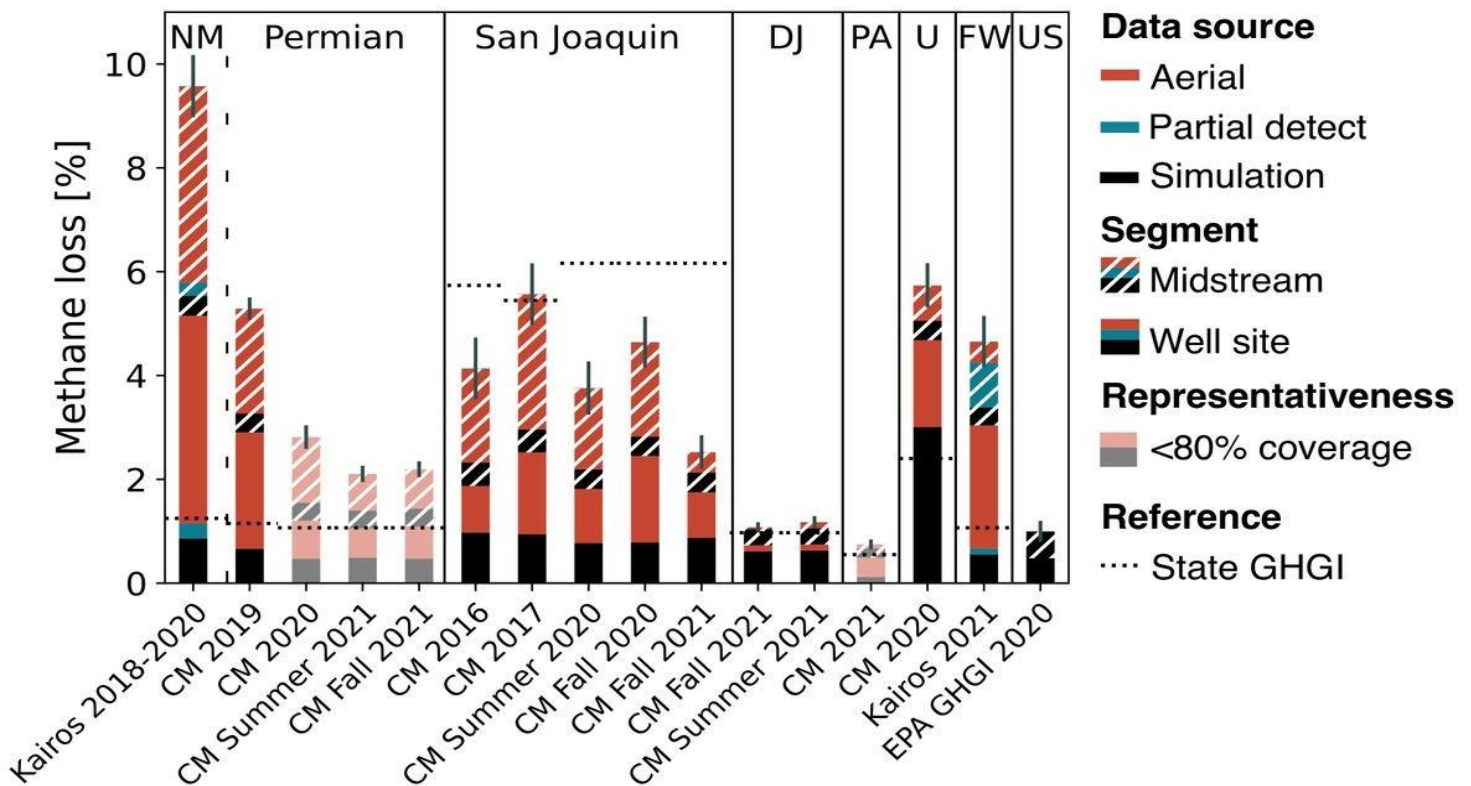
● Well site ● Well site emission ● Midstream emission



Sources: USGS, Flanders Marine Institute, US Census, CEC, Natural Earth, Enverus

Figure 1

A) Surveyed well sites. Remaining active US oil and gas wells in black. B) All aerially detected emissions from well sites (blue) and midstream infrastructure (red). Inset black text denotes total count of well site visits (measurements) for each region, alongside counts of the number of emissions detected from well sites and midstream infrastructure. C) Site-level emission estimation workflow. If emissions are detected during an aerial measurement at a well site, which may contain multiple wells and other equipment, or a midstream asset, that emissions estimate is used directly, after accounting for measurement uncertainty and partial detection probability. If no emission is detected at a well site, we estimate emissions using an emissions simulation tool derived from 5. For midstream assets, we use GHGI simulations to estimate aggregate regional midstream emissions below the aerial detection limit. We also use simulated emissions if an aerially measured emission is below the emission size at which simulated emissions dominate. To characterize uncertainty in total emissions in the surveyed region, we repeat this stochastic process 1000 times for each of the surveyed sites via Monte Carlo analysis, randomly drawing from all aerial



measurements at each site with and, for well sites, without aerially detected emissions. Note that Fort Worth data are not shown in A) and B) to preserve anonymization

Figure 2

Estimated methane loss as a fraction of methane production from oil and natural gas well sites and midstream assets (e.g. pipelines and compressor stations) for all Kairos Aerospace (Kairos) and Carbon Mapper (CM) campaigns in this study in the Permian, San Joaquin, Denver-Julesburg (DJ), Pennsylvania (PA), Uinta (U), and Fort Worth (FW) regions. Colors represent aerially measured emissions (red), implied aerially detectable emissions in the partial detection range (teal, Kairos only), and estimated emissions from component-level simulation (black). Hatched bars represent midstream assets. Dotted lines are corresponding estimates from the Environmental Protection Agency's state-level Greenhouse Gas Inventories, which form the basis for simulated midstream emissions estimates, with the 2020 national estimate for production and midstream displayed in full on the right 9,25. The Kairos Permian campaign covers only the New Mexico Permian, while Carbon Mapper extends into Texas. While most campaigns cover over 80% of total gas production and at least 50% of regional well sites, semi-transparent bars focus disproportionately on high-production areas, which may not have the same emissions profile as the region as a whole. Error bars represent a 95% probability interval, including multiple forms of uncertainty, described in the SI, Section S1.2

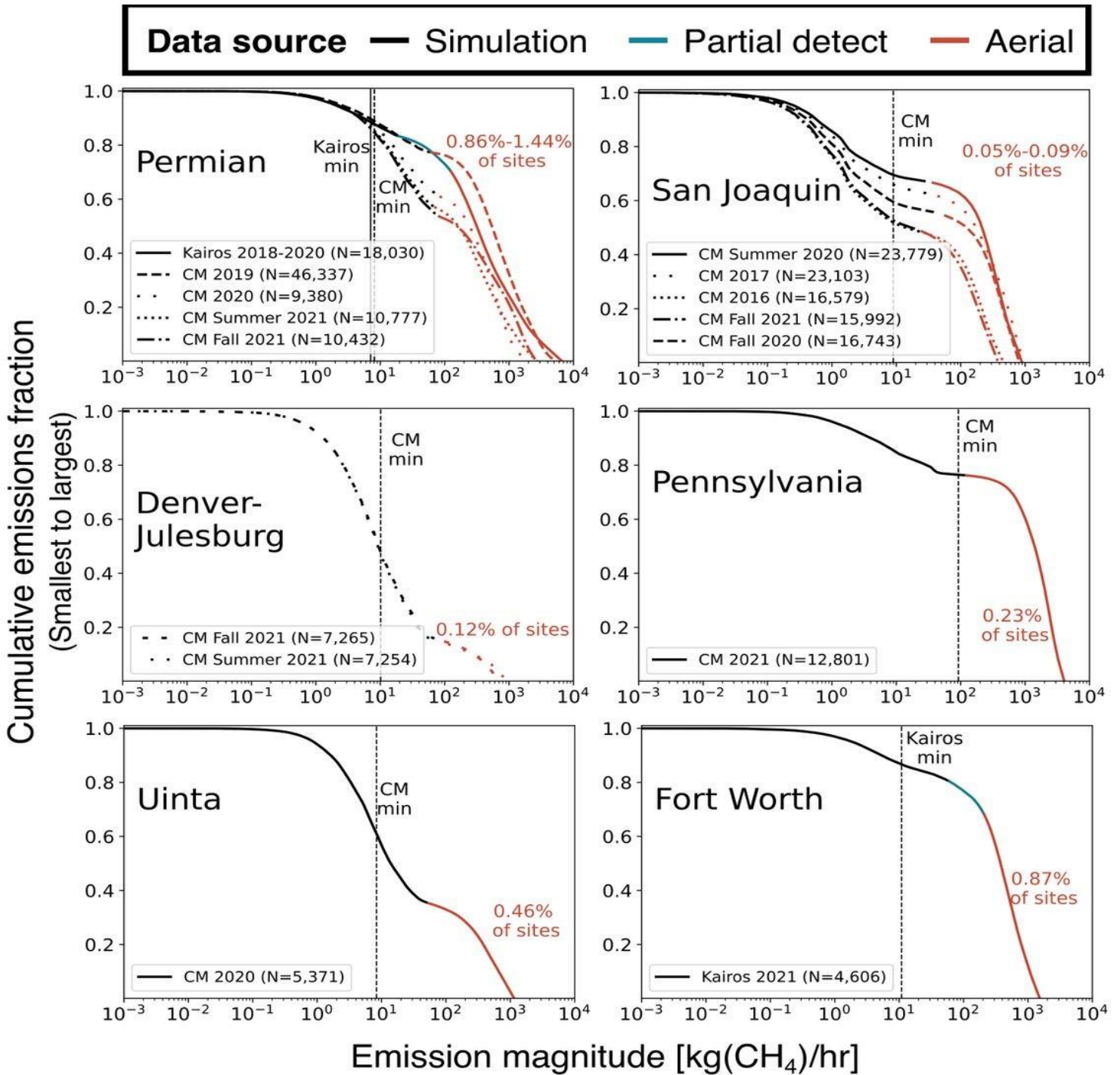


Figure 3

Cumulative well site methane emissions by region. The fraction of total emissions represented by well sites emitting at least a given amount of methane. Red represents direct measurements from aerial campaigns by Kairos Aerospace (Kairos) and Carbon Mapper (CM), with the total number of well sites surveyed listed for each campaign in the legend and fraction of sites with aeriually detected emissions inset. Black represents simulated emissions at surveyed well sites with relatively low emissions. For Kairos campaigns, aerial emissions estimates include a correction for partial detection (teal) for smaller emissions based on single-blind controlled methane release testing. A similar correction for Carbon Mapper is not possible as commensurate blinded and peer-reviewed test data are not yet available. Vertical lines represent the minimum detected emission for each technology in a given region. The transition point away from simulated emissions represents the size beyond which aeriually detected emissions consistently dominate simulated emissions.

REFERENCES

1. Saunio, M. et al. The Global Methane Budget 2000–2017. *Earth Syst. Sci. Data* 12, 1561–1623 (2020).
2. Friedlingstein, P. et al. Global Carbon Budget 2020. *Earth Syst. Sci. Data* 12, 3269–3340 (2020).
3. EPA. Greenhouse Gas Emissions: Understanding Global Warming Potentials. <https://www.epa.gov/ghgemissions/understanding-global-warming-potentials> (2017).
4. US EPA. Inventory of U.S. Greenhouse Gas Emissions and Sinks: 1990-2017. <https://www.epa.gov/sites/production/files/2019-04/documents/us-ghg-inventory-2019-main-text.pdf> (2019).
5. Rutherford, J. S. et al. Closing the methane gap in US oil and natural gas production emissions inventories. *Nat Commun* 12, 4715 (2021).
6. Alvarez, R. A. et al. Assessment of methane emissions from the U.S. oil and gas supply chain. *Science* eaar7204 (2018) doi:10.1126/science.aar7204.
7. Brandt, A. R. et al. Methane Leaks from North American Natural Gas Systems. *Science* 343, 733–735 (2014).
8. Carras, J. N. et al. 2006 IPCC Guidelines for National Greenhouse Gas Inventories. Chapter 4 - Fugitive Emissions. https://www.ipcc-nggip.iges.or.jp/public/2006gl/pdf/2_Volume2/V2_4_Ch4_Fugitive_Emissions.pdf (2006).
9. EPA. Inventory of U.S. Greenhouse Gas Emissions and Sinks: 1990-2020. U.S. Environmental Protection Agency. <https://www.epa.gov/ghgemissions/inventory-us-greenhouse-gas-emissions-and-sinks-1990-2020> (2022).
10. Duren, R. M. et al. California's methane super-emitters. *Nature* 575, 180–184 (2019).
11. Irakulis-Loitxate, I. et al. Satellite-based survey of extreme methane emissions in the Permian basin. *Sci. Adv.* 7, eabf4507 (2021).

12. Cusworth, D. H. et al. Intermittency of Large Methane Emitters in the Permian Basin. *Environ. Sci. Technol. Lett.* 8, 567–573 (2021).
13. Chen, Y. et al. Quantifying Regional Methane Emissions in the New Mexico Permian Basin with a Comprehensive Aerial Survey. *Environ. Sci. Technol.* 56, 4317–4323 (2022).
14. Cusworth, D. H. et al. Strong methane point sources contribute a disproportionate fraction of total emissions across multiple basins in the United States. *Proc. Natl. Acad. Sci. U.S.A.* 119, e2202338119 (2022).
15. Frankenberg, C. et al. Airborne methane remote measurements reveal heavy-tail flux distribution in Four Corners region. *Proc Natl Acad Sci USA* 113, 9734–9739 (2016).
16. Varon, D. J. et al. Satellite Discovery of Anomalously Large Methane Point Sources From Oil/Gas Production. *Geophys. Res. Lett.* 46, 13507–13516 (2019).
17. Varon, D. J. et al. High-frequency monitoring of anomalous methane point sources with multispectral Sentinel-2 satellite observations. *Atmos. Meas. Tech.* 14, 2771–2785 (2021).
18. Lauvaux, T. et al. Global Assessment of Oil and Gas Methane Ultra-Emitters. *Science* 375, 557–561 (2022).
19. Zavala-Araiza, D. et al. Super-emitters in natural gas infrastructure are caused by abnormal process conditions. *Nat Commun* 8, 14012 (2017).